Surface Quality Assessment in Femtosecond Laser Micromachining of Glass under Different Ambient Media

Harish Chandra and Deepak Marla[*]

Department of Mechanical Engineering, Indian Institute of Technology Bombay, Mumbai, 400076, India
[*]Corresponding author's e-mail: dmarla@iitb.ac.in

Femtosecond laser micromachining (FLM) is an effective technique for generating functional surfaces and microfeatures on glass substrates. However, FLM of glass in ambient air is prone to micro-cracks, debris, and thermal damage in the machined region leading to poor surface quality. The ambient medium used in FLM significantly affects the quality of the machined surface. In this study, FLM of glass is carried out in four different ambient media; KOH, HF, DI water, and ethyl alcohol to compare their effects on the surface quality. The glass substrates were submerged 1 mm below the free surface of liquid media and 300 μm wide channels were fabricated by scanning the laser beam of diameter 40 μm and 209 fs pulse duration at variable pulse energies. The experimental results show FLM in KOH solution exhibits better surface quality than HF, DI water, and ethyl alcohol. The surface roughness values of microchannels obtained in the KOH solution were the minimum, measured to be 1.125 μm at 15 μJ. Microcracks were observed in the other three media which were most prominent in ethyl alcohol. FLM of glass in KOH is a promising approach for minimizing roughness and thermal damage without much loss of surface integrity. These findings have implications for the development of glass microfluidic devices and other applications that require precise and functionalized glass surfaces.

1. Introduction

A high transparency along with mechanical and thermal stability make glass a suitable substrate for potential applications in microfluidics [1], MEMS packaging [2], sensors [3]. Microchannels are critical components of a microfluidic system that are used to manipulate tiny amounts of fluids such as mixing and separation. The flow pattern and pressure required depend on the roughness of the surfaces of the microchannels which directly affects the performance of the microfluidic system [4].

The microchannels in glass are fabricated by various techniques but fabrication by femtosecond laser typically involves two steps; direct laser writing and chemical etching. Hong et al. [5] demonstrated laser micromachining of glass with good surface quality. Bai et al. [6] produced 3D glass microfluidic channels using fs laser direct writing and wet etching with HF. Hnatovsky et al. [7] demonstrated the fabrication of microchannels in fused silica and BK7 glass by a femtosecond laser based photoinduced material modification followed by selective chemical etching. Lin et al. [8] fabricated the freeform microchannels of uniform cross-section and length in centimeters using direct fs laser writing followed by selective chemical etching. A similar work was carried out by Yu et al. [9] for fabrication of low-loss optical waveguides in fused silica using a spatially shaped femtosecond laser followed by selective chemical etching. The fabrication of microchannels in glass by a femtosecond laser followed by post-chemical etching involves two steps and is time-consuming [10].

The microchannels in glass can be generated by femtosecond laser micromachining (FLM) in a single step. FLM of glass in ambient air has been reported on depth control of microchannels [11] but due to brittleness and poor thermal conductivity, the FLM of glass in ambient air leads to common defects such as debris, micro-cracks, chippings, and thermal damage that lead to poor surface quality [5, 12, 13]. Xu et al. [14] demonstrated that the introduction of water in femtosecond laser direct writing improved the ablation efficiency. The presence of liquid medium above the glass substrate confines plasma-induced ablation, and increases penetration depth into the substrate which in turn improves the ablation efficiency of the laser [15-17]. However, there is a limited research reported on the use of different ambient media on the surface quality of microchannels fabricated by FLM. The fabrication of microchannels with good surface characteristics using FLM without chemical etching remains challenging. This study introduces different liquid media in FLM to produce microchannels on glass surfaces. The FLM of glass was carried out under different ambient media, and a comparative study has been presented to assess the surface quality of microchannels in KOH, HF, DI water, and ethyl alcohol.
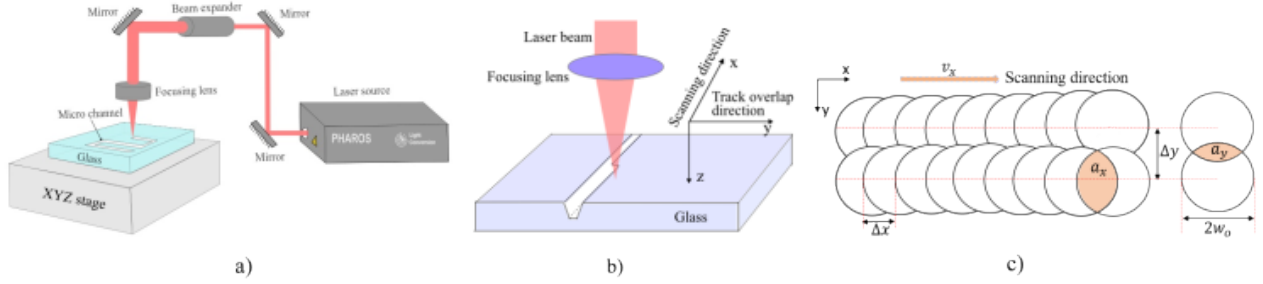
2. Materials and methods
2.1 Materials

A quartz glass sheet of 0.55 mm thickness was used as a substrate to ablate the surface with a fs laser using single and multiple fs pulses. The air and four liquids, viz., KOH, HF, DI water and ethyl alcohol were used as ambient media. The glass substrates were first processed with fs laser in ambient air, and then processed in the other four media to produce craters, grooves, and microchannels and compare their quality. The concentration of the chemical etchants was kept constant for all the experiments equal to 50% (w/w). The material of the containers used was chemically inert to all the ambient media used. The machined glass substrates were

cleaned with acetone to remove chemicals and contaminants.

2.2 Experimental setup

A femtosecond laser (PHAROS, Light conversion) with a wavelength of 1030 nm, maximum pulse energy of 200 µJ, and a pulse duration of 206 fs was used to carry out all the experiments for producing the craters, single line grooves, and microchannels on the glass substrate at variable process parameters. A focusing lens of 122 mm focal length was used to obtain a beam spot diameter of 40 µm. A 3-axis CNC stage was used to control the motions and pulse overlaps along x- and y-directions.

$$\theta_y = \cos^{-1}\left(\frac{\Delta y}{2w_o}\right), \tag{4}$$

where, a_x and a_y are areas of intersection along x and y-directions respectively, w_o is the beam spot radius, θ_x and θ_y are arbitrary variables, Δx and Δy are spot pitch and hatch distance, respectively i.e. distances between centers of two adjacent overlapping pulses along x and y-directions, respectively (see Fig. 1 (c)), v_x is scanning speed along x-direction, and f is pulse repetition rate. The percentage of area overlaps of pulses along the y-axis are 96.82%, 84.13%, and 68.5% corresponding to 1, 5, and 10 µm hatch distances, re-

Fig. 1 a) Schematic of the experimental setup, b) scanning strategy used, c) a_x and a_y are areas of intersection along x and y axes.

The laser beam has a Gaussian profile with an exit diameter of 3.67 mm which was expanded to 9 mm using a variable beam expander (as shown in Fig. 1 (a)). A DC-powered mini-centrifugal pump was used to constantly supply liquid which was uniformly spread, by a rectangular splitter connected to the circular pipe of the pump, in the form of a thin layer over the glass surface subject to direct laser ablation. A constant and uniform flow of the thin layer of the liquid medium over the glass substrate was maintained. The submerged sample was irradiated with a femtosecond laser to produce single and multi-pulse craters, and grooves, and microchannels using multiple scans. Two different features were produced by scanning the laser in different media. Grooves were generated by scanning the laser beam at a constant scan speed of 10 mm/s, pulse repetition rate of 200 kHz and varying pulse energy from 15 to 40 µJ. Microchannels were produced using multiple scans with hatch distance varied from 1 to 10 µm. All the experiments were carried out under room temperature and pressure of 25°C and 1 atm respectively.

2.3 Scanning method

The laser beam was scanned along the x-axis and fed along the y-axis at variable hatch distance to produce microchannels on glass substrates (see Fig. 1 (b)). The fractions of area overlap of pulses along x and y-directions are defined as φ_x and φ_y, which can be computed from the following equations (see Fig. 1 (c)),

$$\varphi_x = \frac{a_x}{\pi w_o^2} = \frac{1}{\pi}(2\theta_x - \sin 2\theta_x), \tag{1}$$

$$\varphi_y = \frac{a_y}{\pi w_o^2} = \frac{1}{\pi}(2\theta_y - \sin 2\theta_y), \tag{2}$$

$$\theta_x = \cos^{-1}\left(\frac{\Delta x}{2w_o}\right) = \cos^{-1}\left(\frac{v_x}{2w_o f}\right), \tag{3}$$

spectively. The area overlap is a key parameter that has a direct impact on the depth of the craters and grooves. The hatch distance, which is the distance between the centers of two scans along y-axis, was varied from 1 to 10 µm to produce different microchannels of 300 µm width under different ambient media.

2.4 Characterization

The quality of micromachined surfaces was quantified in terms of the average roughness value Sa, the presence of microcracks at the edges, and the presence of thermal damage along the edge of the microchannel. An optical microscope (Zeta, Model 20) was used to measure the depth, width, and profile of the craters and microchannels. The roughness of the bottom surface of microchannels was measured using an optical microscope. Further scanning electron microscopy (Zeiss Ultra 55) was used to closely examine the surface and edge quality, microcracks, debris, and thermal damage in the microchannels fabricated in KOH solution and other liquid media (as shown in Fig. 11 below).

3. Results and discussions

The preliminary experiments of single and multi-pulse ablation were conducted on a glass substrate in the ambient air and other ambient media to study, and compare the variation of the crater depth and width with laser fluence and overlap ratio. The working fluence for the fabrication of the grooves using single and overlapping lines was selected from the defect parameters. The selected process parameters were used for the micromachining of glass under different ambient conditions and comparison of results.

3.1 Single and multi-pulse ablation in ambient air

The glass samples were irradiated with femtosecond laser pulses using a wide range of pulse energy. The width of

the crater increased with the increasing number of pulses from 1 to 500 at a constant pulse energy of 200 µJ (see Fig. 2) and pulse energy from 20 to 200 µJ at a constant number of pulses (see Fig. 4). The increase of pulse energy well above multipulse-threshold fluence resulted in a greater increase in depth than in width which can be observed in the profile curves of craters (as shown in Fig. 3 (a) and (b)). Further, double-line groves were engraved on the glass using a laser spot diameter of 40 µm and fluence level from 1.2 to 3.98 J/cm² obtained from single and multipulse ablation experiments in ambient air. At higher fluence above 3.98 J/cm², the chipping and microcracks were observed, along the edge of the grooves similar to those observed in craters, due to the high -temperature gradient between irradiated volume and
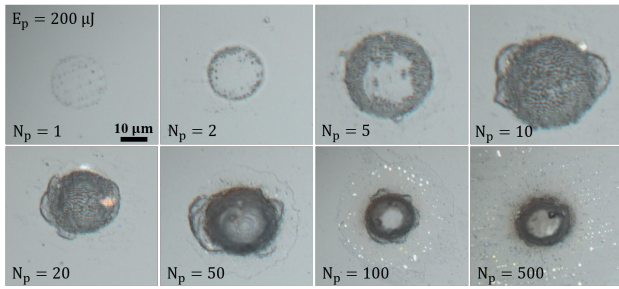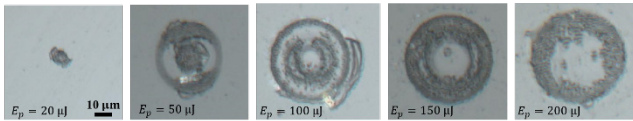

Fig. 2 Microscopic images of craters at different pulse number and a constant pulse energy of 200 µJ.
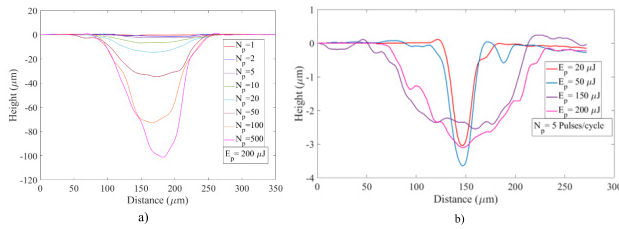
Fig. 3 a) Effect of the number of pulses each with energy of 200 µJ on crater profiles, b) effect of pulse energy as a burst of five pulses on crater profiles.

surrounding material. The laser fluence in the range of 1.2-3.98 J/cm² was used for further experiments using multiple scans.

Fig. 4 Microscopic images of craters at different pulse energies at a constant pulse number of 5.

3.2 Effect of liquid medium in FLM

The quartz glass sample was submerged 1 mm below the thin layer of the liquid medium flowing at a constant rate of 240 ml/min. The submersion of the sample under a thin layer of liquid resulted in the change of the position of the laser focal spot due to refraction. Subsequently, the laser beam undergoing refraction causes a shift in focal spot by a depth δ for a low intensity and thin layer of liquid [13]. The approximate shift (δ) of the laser focal spot, into the substrate submerged at a very small depth h in the liquid (see Fig. 5 (b)), is computed from the following equation derived from Snell's law,
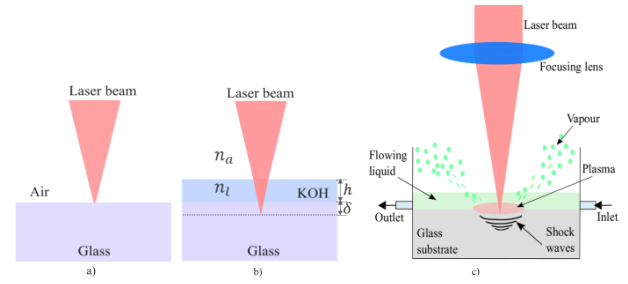
Fig. 5 Effect of ambient media on the position of focal spot a) air b) KOH, c) fs laser micromachining of glass in liquid medium.

$$\delta \approx h \left(\frac{n_l}{n_a} - 1 \right), \tag{5}$$

where, n_l and n_a are refractive indices of liquid and air, respectively. The approximate shift of focal spot was 0.407 mm corresponding to 1 mm thick layer of the liquid above the glass surface. The absorption of the laser energy in the liquid results in the formation of vapor and cavitation bubbles which are carried away by the flowing liquid layer. A major part of the incident laser energy penetrates the glass substrate and results in optical breakdown. At higher fluence, a plasma is generated near the glass-liquid interface and is followed by the generation of the shockwaves [16] (see Fig. 5 (c) above). The pressure of shock waves results in the formation of a thin and hard densified silica layer in the craters and grooves [18]. The densified silica in the craters and grooves gets dissolved in the flowing liquid. However, the solubility of the densified silica depends on the type of ambient medium and its concentration. In addition, the temperature of the irradiated and localized volume in the glass increases drastically which greatly affects the solubility of the densified silica in the liquid medium. As a result, the densified silica layer in the craters or grooves gets partially or fully dissolved and carried away by the flowing liquid. The resulting craters or grooves are free of debris as compared to those obtained in the ambient air.

3.3 Crater profiles in ambient air and KOH

The multipulse ablation experiments were carried out to analyze the effect of ambient air and 50% (w/w) KOH solution at constant laser parameters. The craters were produced by using a burst of 500 pulses each with an energy of 200 µJ and pulse width of 206 fs. The etching rate of the KOH solution increases with the temperature of the irradiated volume [19]. The temperature of the irradiated and localized volume in the glass rises drastically which triggers the rapid etching without any external heat source. As a result, the densified silica layer in the craters or grooves gets dissolved in and carried away by the flowing KOH solution.

In addition to this, etching with KOH has high resistance to thermal damage and cracks [20]. As a result, the crater produced in the KOH solution has a higher depth with minimum thermal damage around the edge (see Fig. 7). On the other hand, a haze band due to loss of transparency is formed around the edge of the crater formed in the air (as highlighted in Fig. 6) while in KOH no haze band is observed.
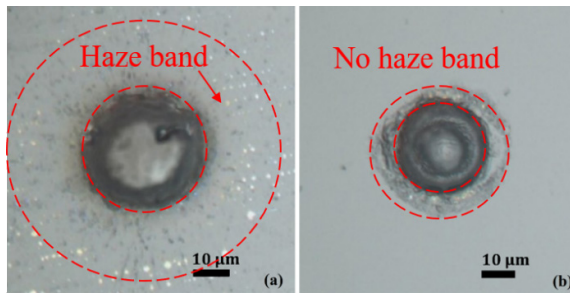
**Fig. 6** SEM images of FLM surfaces obtained in (a) air (b) 50% KOH.
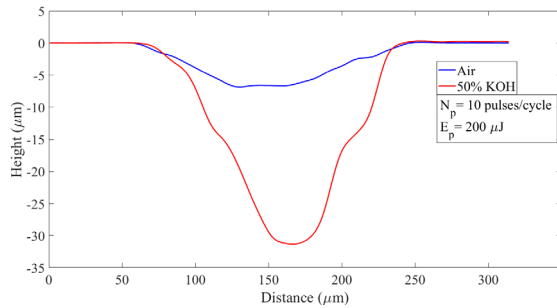
Fig. 7 Surface profiles of craters generated in air and KOH using 10 pulses each with an energy of 200 **μ**J.

3.4 Overlapping grooves in KOH

The two overlapping single-line grooves were produced at a variable hatch distance of 1-10 μm by irradiating glass substrate in KOH solution. The maximum pulse energy was selected at 40 μJ to minimize thermal damage to the edges of the grooves. The pulse energy was varied in the range of 15-40 μJ to study the effect of overlap and fluence on the depth and width of the microchannels. The silica rich white bands were formed along the length of channel at a hatch distance of 10 μm and area overlap of 68.5%. In this case, a shallow channel was produced. The effect of area overlap in terms of hatch distance on the surface and edge quality of grooves produced by two overlapping scans, is shown in Fig. 8. The microgrooves were deepest and narrowest corresponding to 1 μm hatch distance and an area overlap of 96.82%. The depth and width of all the groves increased with increasing fluence and subsequently, the aspect ratio also increased with fluence for a given overlap ratio (see Figures 9 (a) and (b)).
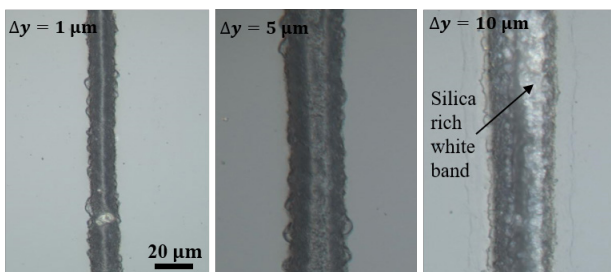

Fig. 8 Double-scanned grooves produced at hatch distances of 1, 5 and 10 **μ**m along the width.
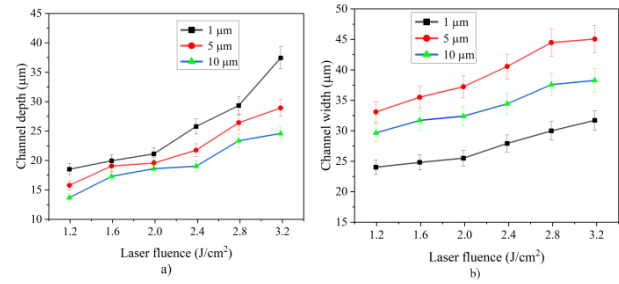


Fig. 9 a) Depth of grooves created by overlapping of two scans at different hatch distances, 1, 5, and 10 μm, b) width of grooves created by overlapping of two scans at different hatch distances of 1, 5, and 10 μm.

3.5 Fabrication of microchannels in different media

Based on the results obtained from the overlapping of two lines as discussed in section 3.4, a hatch distance of 5
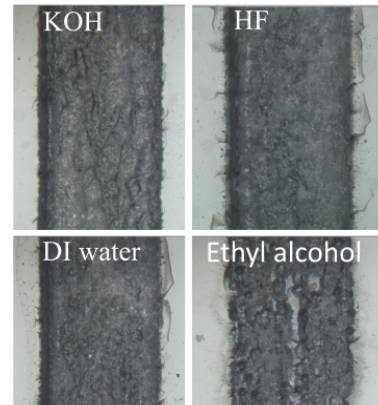

Fig. 10 Microchannels fabricated in different ambient media.
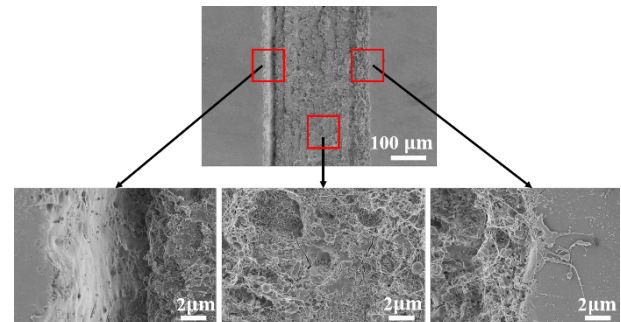
Fig. 11 SEM images of microchannel fabricated in KOH.

μm and an area overlap of 84.13% was selected for a minimum taper and smooth surface of grooves. The microchannels of a constant width of 300 μm were fabricated at a constant hatch distance of 5 μm and variable pulse energy from 15 to 40 μJ to study the effect of fluence in different liquid media; KOH, HF, DI water, and ethyl alcohol. The high-intensity femtosecond pulsed laser with IR-wavelength of 1030 nm, generates localized heating and ionization through
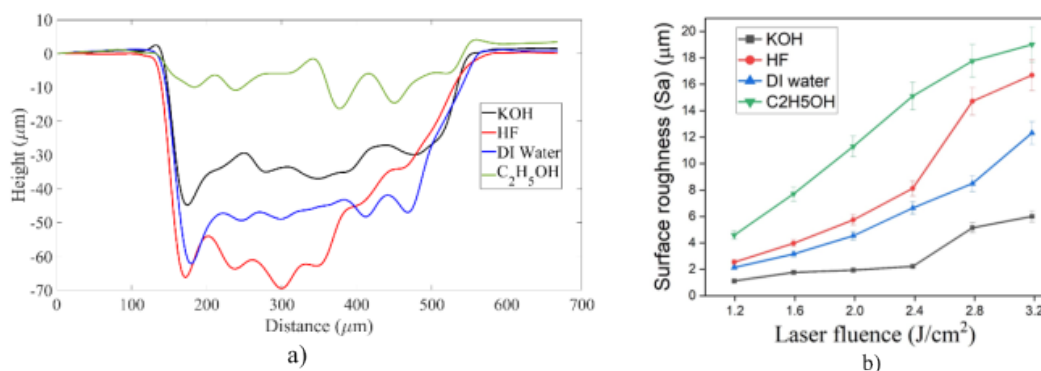
Fig. 12 a) Profile curves for microchannels in different media, b) Roughness of bottom surface of microchannels for different ambient media.

non-linear absorption in glass. KOH and HF are good chemical etchants for glass. When both of these etchants are introduced in direct laser ablation, the etching rate of glass increases rapidly due to localized heat generation in the absorbed volume. As a result, material removal takes place in a controlled manner in both the etchants. The channels produced in KOH were free of microcracks due to high crack resistance and laser damage threshold of KOH [20]. On the other hand, DI water, and ethyl alcohol are non-reactive to glass. The introduction of these two media in direct laser ablation removes the silica-rich ablated material and dissipates the localized heat generated in the glass. However, the microcracks at the edges and surface or subsurface damages were observed in the microchannels fabricated in HF, DI water, and ethyl alcohol (see Fig. 10). The SEM image at high magnification showed that there was no evident defect in the microchannels fabricated in the KOH solution (see Fig. 11).

The profile of the microchannel obtained in the KOH solution is more uniform and straight as compared to that in other three media (as shown in Fig. 12 (a)). The roughness of the surface obtained in different ambient media increased with increasing fluence and was found to be minimal in the KOH solution (see Fig. 12 (b)). The higher damage resistance of KOH solution produced defect-free microchannels in the glass with good overall surface and edge quality [21].

Conclusions

This study presents a comparative analysis of the surface quality of microchannels fabricated on glass under various ambient media using femtosecond laser micromachining. The experimental results demonstrate that micromachining in a KOH solution improves the surface quality of glass with edges free from laser-induced defects. The optimal surface roughness of 1.125 μm was achieved at a fluence of 1.2 J/cm² and a hatch distance of 5 μm in 50% KOH solution. The work highlights KOH's superior potential for enhancing glass damage resistance compared to the more commonly used HF etchant. Additionally, the overlap ratio of laser pulses plays a critical role in reducing surface roughness, which can be further minimized to submicron levels through careful optimization of laser parameters. The findings underscore the importance of selecting appropriate media and laser parameters to achieve optimal results in femtosecond laser micromachining.

References
[1] J.M. Acosta-Cuevas, M.A. García-Ramírez, G. Hinojosa-Ventura, Á.J. Martínez-Gómez, V.H. Pérez-Luna, and O. González-Reynoso: Coatings, 13, (2023) 1676.
[2] K. Garasz, M. Kocik, M. Tański, R. Barbucha, J. Mizeraczyk, M. Nejbauer, and C. Radzewicz: Proc. SPIE, Vol. 8902, (2013) 442.
[3] F. He, Y. Liao, J. Lin, J. Song, L. Qiao, Y. Cheng, and K. Sugioka: Sensors, 14, (2014) 19402.
[4] B. Nasseri, S. Akar, and E. Naseri: "Biomedical Applications of Microfluidic Devices," ed. by Academic Press, (Elsevier, Amsterdam, 2021) p.37.
[5] M.H. Hong, K. Sugioka, D.J. Wu, L.L. Wong, Y. Lu, K. Midorikawa, and T.C. Chong: Proc. SPIE, Vol. 4637, (2002) 270.
[6] S. Bai, D. Serien, A. Hu, and K. Sugioka: Adv. Funct. Mater., 28, (2018) 1706262.
[7] C. Hnatovsky, R.S. Taylor, E. Simova, P.P. Rajeev, D.M. Rayner, V.R. Bhardwaj, and P.B. Corkum: Appl. Phys. A, 84, (2006) 47.
[8] Z. Lin, J. Xu, Y. Song, X. Li, P. Wang, W. Chu, Z. Wang, and Y. Cheng: Adv. Mater. Technol., 5, (2020) 1900989.
[9] J. Yu, J. Xu, Q. Dong, J. Qi, J. Chen, A. Zhang, Y. Song, W. Chen, and Y. Cheng: Opt. Laser Technol., 158, (2023) 108889.
[10] R. Fiorin, L.N. da Costa, I. Abe, I. Chiamenti, C.C. de Moura, and H.J. Kalinowski: Proc. IEEE MTT-S Int. Microwave & Optoelectron. Conf., (2013) 1.
[11] A. Rodríguez, A. Arriola, T. Tavera, N. Pérez, and S.M. Olaizola: Microelectron. Eng., 98, (2012) 672.
[12] Y. Wang, B. Xia, S. Han, C. Li, and L. Wan: Processes, 10, (2022) 1309.
[13] J.S. Hoppius, S. Maragkaki, A. Kanitz, P. Gregorčič, and E.L. Gurevich: Appl. Surf. Sci., 467, (2019) 255.
[14] J. Xu, D. Wu, J.Y. Ip, K. Midorikawa, and K. Sugioka: RSC Adv., 5, (2015) 24072.
[15] E. Markauskas, L. Zubauskas, G. Račiukaitis, and P. Gečys: Micromachines, 14, (2023) 176.
[16] T. Sato: "High-Energy Chemistry and Processing in Liquids," ed. by Springer Nature Singapore, (Springer, Singapore, 2022) p.187.

[17] S. Zhu, Y.F. Lu, M.H. Hong, and X.Y. Chen: J. Appl. Phys., 89, (2001) 2400.

[18] H. Hu, X. Wang, and H. Zhai: J. Phys. D: Appl. Phys., 44, (2011) 135202.

[19] M. Noor, B. Bais, and B.Y. Majlis: Proc. IEEE Int. Conf. Neural Inf. Process., (2002) 524.

[20] L. Sun, T. Shao, X. Zhou, F. Li, S. Chen, W. Li, X. Ye, et al.: Opt. Mater., 108, (2020) 110249.

[21] M. Pfiffer, P. Cormont, E. Fargin, B. Bousquet, M. Dussauze, S. Lambert, and J. Neauport: Opt. Express, 25, (2017) 4607.